

Evidence of nodal superconductivity in LaFeSiH

A. Bhattacharyya,¹ P. Rodière,² J.-B. Vaney,³ P. K. Biswas,⁴ A. D. Hillier,⁴ F. Bernardini,⁵ S. Tencé,³ D.T. Adroja,^{4, 6, *} and A. Cano^{2, †}

¹*Department of Physics, Ramakrishna Mission Vivekananda Educational and Research Institute, Belur Math, Howrah 711202, West Bengal, India*

²*Institut Néel, CNRS & Univ. Grenoble Alpes, 38042 Grenoble, France*

³*ICMCB, CNRS & Université Bordeaux, UPR 9048, F-33600 Pessac, France*

⁴*ISIS Neutron and Muon Facility, SCFT Rutherford Appleton Laboratory, Chilton, Didcot Oxon, OX11 0QX, United Kingdom*

⁵*Dipartimento di Fisica, Università di Cagliari, IT-09042 Monserrato, Italy*

⁶*Highly Correlated Matter Research Group, Physics Department, University of Johannesburg, PO Box 524, Auckland Park 2006, South Africa*

(Dated: April 3, 2022)

Unconventional superconductivity has recently been discovered in the first iron-based superconducting silicide LaFeSiH. By using the complementary techniques of muon spin rotation, tunneling diode oscillator and density functional theory, we unveil the nodal character of the superconducting gap of this novel high-temperature superconductor. Even if the topology of the computed Fermi surface is compatible with the s_{\pm} -wave case with accidental nodes, its nesting and orbital-content features may eventually result in a d -wave state, more unusual for high-temperature superconductors of this class.

INTRODUCTION

The superconducting energy gap is a hallmark of superconductivity at the level of the electronic structure [1]. Furthermore, the symmetry of the gap function is intimately linked to the microscopic interactions that yield the Cooper pairing, thus providing key information about the mechanism behind superconductivity. Iron-based superconductors have proven to be a distinct class of unconventional superconductors [2] in which the gap symmetry can be tuned by means of external control parameters such as doping, pressure, or disorder [3, 4]. In view of their distinct multiband features, it was soon realized that the so-called s_{\pm} -wave gap with a sign change between electron and hole pockets in the Fermi surface is the natural candidate for the gap function in most of these materials [5]. In this case, doping, for example, can lead to enhanced anisotropy by means of various effects such as the modification of intraband Coulomb interactions and changes in the orbital weights on the Fermi surface. At the same time, it was also realized that the d -wave pair channel is a strong competitor to the s_{\pm} -wave one [6]. In this case the key role is played by the hole pockets where the gap function displays symmetry-imposed nodes. In fact, a strong tendency towards d -wave pairing, even dominating over the s -wave one, has been found in various models suited for 1111 systems, especially towards the overdoped limit [6–8]. These considerations explain the general trends observed in the Fe-based superconductors, including the controlled changes reported in BaFe₂(As,P)₂ [9] and (Ba,Rb)Fe₂As₂ [10].

Here, we investigate the gap structure of the novel superconductor LaFeSiH with $T_c \sim 10$ K in its parent phase [11]. This system is the first silicide in the family of Fe-based superconductors, whose unconven-

tional mechanism of superconductivity is yet to be elucidated [12]. Compared to LaFeAsO, the topology of the Fermi surface is essentially preserved in LaFeSiH at the expense of an increased 3D character that reduces considerably the nesting. To determine the properties of the corresponding superconducting gap we measured the magnetic penetration depth λ . The temperature dependence of this fundamental quantity maps the excited quasiparticles, and hence the structure of the superconducting gap. Specifically, we performed muon spin rotation and relaxation (μ SR) experiments and used tunnel diode oscillators (TDO) to determine λ . Details are provided in the Methods section. While the μ SR technique provides a direct access to λ by probing the magnetic field distribution in the vortex state [13, 14], the TDO method enables the collection of a large density of points with very high resolution, and hence a very precise determination of the changes in λ in the Meissner state [15]. These complementary techniques are supplemented with density-functional-theory (DFT) calculations, from which we compute the zero-temperature penetration depth $\lambda(0)$ in the London approximation and rationalize the nodal behavior observed in our measurements as a function of temperature.

RESULTS

μ SR experiment

Fristly, we report the μ SR experiment. Figs. 1 (a) and (b) show the transverse-field μ SR (TF- μ SR) asymmetry spectra measured in the normal state of LaFeSiH at 20 K and in the superconducting state at 0.3 K. The damping of the asymmetry oscillations observed in the normal state is very small, which indicates that these oscillations are mainly due to nuclear contributions with a distribution of the internal field that is extremely uniform for

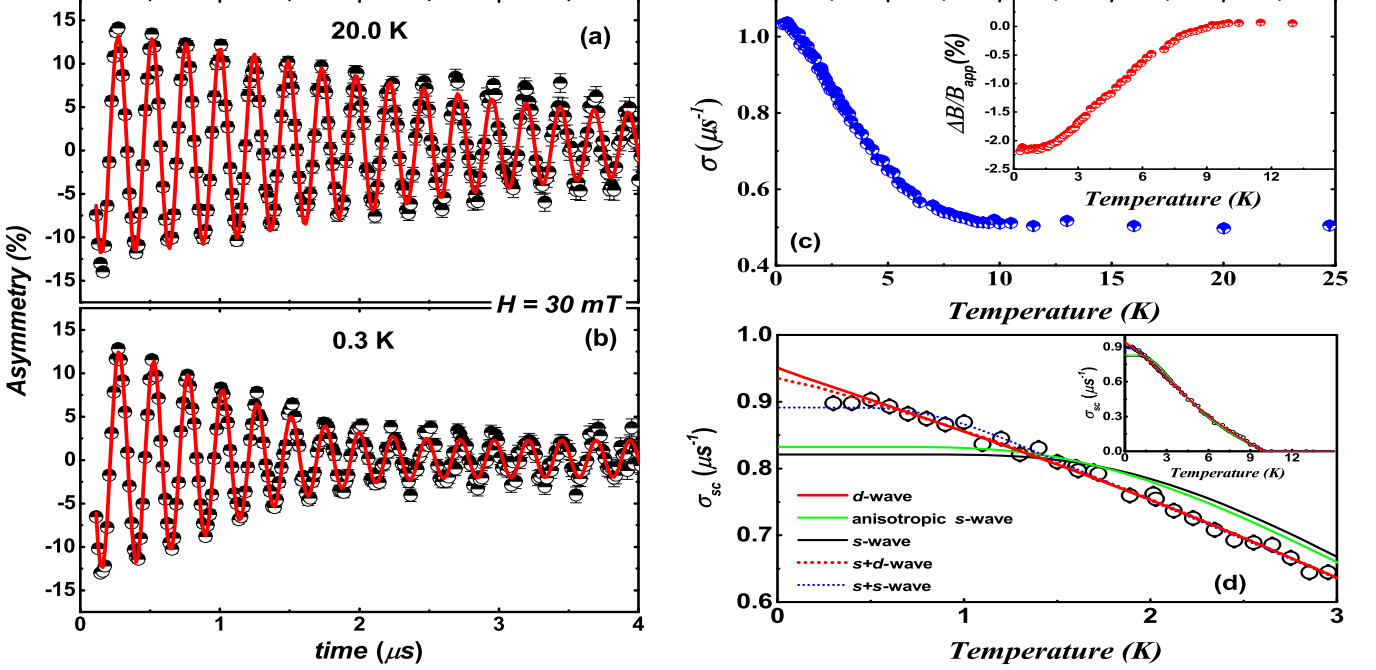


FIG. 1. TF- μ SR asymmetry spectra for LaFeSiH collected at $T = 20$ K (a) and at $T = 0.3$ K (b) at an applied magnetic field of $H = 30$ mT. The solid line shows a fit using Eq. (1). (c) Temperature dependence of the total muon depolarization rate σ . The inset shows the normalised internal field $\Delta B(T)/B_{\text{app}} = [B(T) - B(T = 20\text{ K})]/B_{\text{app}}$, where $B(T) = \gamma_\mu \omega_s(T)$. (d) Superconducting contribution to the muon depolarization rate $\sigma_{\text{sc}}(T)$ as a function of temperature up to 3 K. The lines are the fits to the data using Eq. (2) for various gap models. Among the single-gap models, the best fit is obtained with the *d*-wave model. If a second gap is included, then the *s* + *d*-wave model provides the best fit. The data in the full temperature range that includes the normal state ($T_c \simeq 10$ K) is shown in the inset.

the applied field. In the superconducting state, in contrast, the damping is substantially higher, as expected from inhomogeneous field distribution created by the superconducting vortices.

The red lines in Fig. 1 (a) and (b) illustrate the fits of the TF- μ SR data according to Eq. (1). The parameters θ and $A_{bg} = 0.18$ were estimated by fitting to the 20 K and 0.3 K data respectively and their values were kept fixed in the fitting of the other temperature data points. The parameters A_s and ω_{bg} were allowed to vary, which nevertheless resulted in nearly temperature-independent parameters. The good agreement of the fits validates the model Eq. (1).

The total depolarization rate σ as a function of temperature is shown in Fig. 1(c). The clear increase from $\sigma = \sigma_{\text{nm}} = 0.508(1)$ with decreasing temperature confirms the emergence of superconductivity in LaFeSiH. This can additionally be concluded from the substantial decrease in the internal field shown in the inset of Fig. 1(c). The estimated superconducting contribution σ_{sc} is shown in Fig. 1 (d). The T_c derived from this data is $\simeq 10$ K, which is slightly higher than the onset observed in the DC magnetic-response measurements on the same samples (see also [11]). Since μ SR has much higher sensitivity with respect to the superconducting volume

fraction, this suggests that there is a non-negligible distribution of T_c 's within the sample.

The zero-temperature penetration depth $\lambda(0)$ can be directly determined from the TF- μ SR parameter σ_{sc} . The extrapolation of σ_{sc} to zero temperature gives $\lambda(0) = 336$ nm, which is similar to that reported in other Fe-based superconductors. This quantity, however, has to be understood as the effective penetration depth λ_{eff} which, in powder samples of very anisotropic layered compounds, can be expected to be dominated by the in-plane penetration depth λ_{ab} . That is, $\lambda_{\text{eff}} \approx 3^{1/4} \lambda_{ab}$ [16] so that $\lambda_{ab} \approx 255$ nm. These values can also be compared with the values expected according to the specific band structure of LaFeSiH. The computed values are reported in Table I, which are perfectly compatible with the zero-temperature penetration depth estimated from the μ SR data.

Fig. 1(d) shows the fits of $\sigma_{\text{sc}}(T)$ according to Eq. (2) for different models of the superconducting gap (the fitting parameters are summarized in Table II). Among the one-gap models, the best fit is obtained for the model with *d*-wave symmetry of the superconducting gap. In fact, compared to the *s*-wave models, the *d*-wave one reproduces much better the low-temperature behavior [see Fig. 1(d)]. The overall fit improves slightly by con-

FS sheet	$\langle \frac{v_x^2}{v_F} \rangle$ [km/s]	$\langle \frac{v_z^2}{v_F} \rangle$ [km/s]	$\lambda_x(0)$ [nm]	$\lambda_z(0)$ [nm]
1	51	12	323	698
2	63	5	266	951
3	53	66	207	186
4	79	18	145	305
5	110	10	226	759

TABLE I. Zero-temperature magnetic penetration length of LaFeSiH obtained from DFT calculations in the London approximation. The different rows indicate the values obtained from each Fermi-surface sheet, labelled as in Fig. 3 (sheets 1-3 and 4-5 correspond to the hole-like and electron-like pockets respectively in the $k_z = 0$ plane, i.e. around Γ and M). $\langle v_i^2/v \rangle \equiv \frac{1}{S_n} \oint dS_n (v_i^2/v)$, where S_n is the corresponding Fermi-surface area.

Gap model	$g(\phi)$	Δ_0 (meV)	weight factor	χ^2
<i>d</i> -wave	$\cos(2\phi)$	1.22	1	1.20
anisotropic <i>s</i> -wave	$\frac{ 1+\cos(4\phi) }{2}$	1.03	1	3.95
<i>s</i> -wave	1	0.84	1	4.77
<i>s</i> + <i>d</i> -wave	1, $\cos(2\phi)$	1.09; 0.66	0.66; 0.34	1.04
<i>s</i> + <i>s</i> -wave	1	1.04; 0.36	0.32; 0.68	1.10

TABLE II. Values of the fitting parameters obtained from the $\sigma_{sc}(T)$ fit for different gap structures. $T_c = 10.0(2)$ K was estimated from *s*-wave fit and kept fixed in all other fits.

sidering two-gap models, although in this case too the best fit is obtained when the model includes a *d*-wave component. Thus, the TF- μ SR data gained on LaFeSiH, and in particular its low-temperature behavior, suggests a superconducting gap with *d*-wave symmetry.

We note, however, that the fits of the TF- μ SR data yield gap values that are systematically below the BCS weak-coupling limit. For the *d*-wave model for example the gap parameter becomes $\Delta_d = 1.41k_B T_c$, while the *s* + *d*-wave model gives $\Delta_s = 1.30k_B T_c$ and $\Delta_d = 0.57k_B T_c$, both below their corresponding BCS weak-coupling limit. Since these parameters turn out to be unphysical, the TF- μ SR analysis reveals that there is an additional ingredient playing a role.

TDO measurements

In order to clarify the situation we performed additional TDO measurements. In Fig. 2 (a) we show the AC magnetic susceptibility measured in LaFeSiH as a function of the temperature for these two configurations. The perfect diamagnetic behavior observed in both cases confirms the superconducting transition with onset $T_c \approx 10$ K. In the normal state above T_c , the TDO signal becomes constant, which reveals that the skin depth is larger than the size of the sample. From this data, the normal-state resistivity is estimated as $> 20 \mu\Omega$ cm in all the measured samples.

The magnetic susceptibility displays essentially the same behavior as a function of the temperature irrespec-

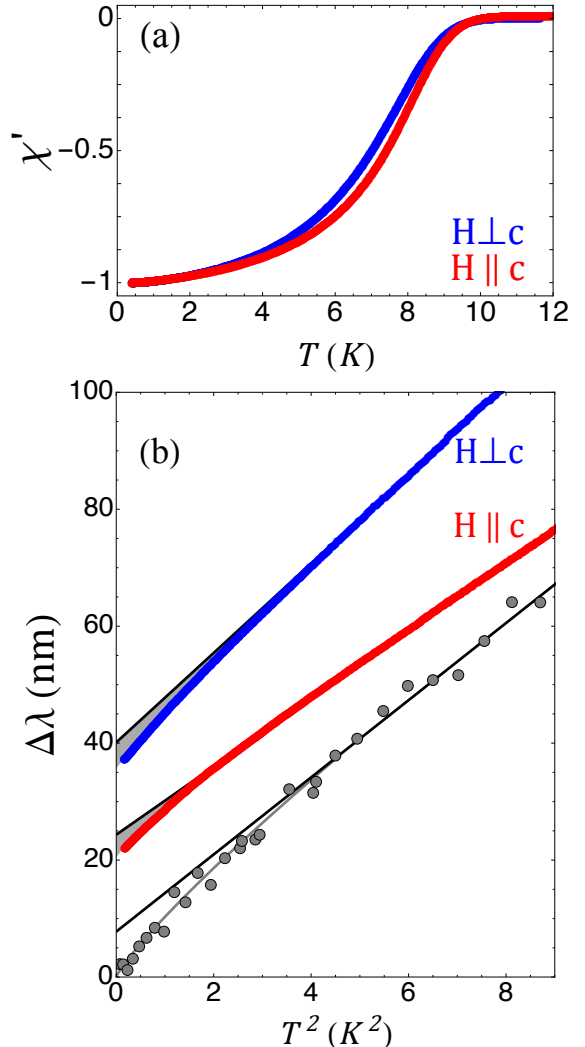


FIG. 2. Magnetic response measured in single-crystal LaFeSiH. (a) AC susceptibility across the superconducting transition ($T_c \approx 10$ K) with the magnetic field applied along the c -axis (red) and in the basal ab -plane (blue). (b) Change in the magnetic penetration depth $\Delta\lambda$ against T^2 in the low-temperature region below $T_c/3$. TDO data is in red for $H \parallel c$ and in blue for $H \perp c$, while the gray circles correspond to the μ SR data. The TDO data has been normalized according to the μ SR data and a vertical offset has been introduced for clarity. Black lines are T^2 fits above 2.5 K. The two data sets clearly follow a power-law T^n behavior with $n < 2$ at low temperatures, revealing the presence of line nodes in the superconducting gap.

tive of the direction of the applied field. This suggests that the anisotropy between in-plane and out-of-plane superconducting properties is such that $\Delta\lambda_{ab} > \Delta\lambda_c/30$, so that the signal is always dominated by $\Delta\lambda_{ab}$ due to the aspect ratio of the samples ($d/w \sim 1/30$). This is in fact in tune with the weak anisotropy obtained in our DFT calculations (see Table I). At the same time, the quantitative agreement between the susceptibility for the two orientations of the magnetic field is rather surprising.

Also, the drop across the transition is quite broad indicating again a non-negligible distribution of T_c 's. These features suggest that the effective geometrical factors are more complex in these samples.

Fig. 2 (b) shows the measured changes in the magnetic penetration depth as a function of T^2 in the low-temperature limit. The data clearly follows a power law T^n with an exponent $n < 2$, which is a strong indication of line nodes in the superconducting energy gap [4, 15]. Specifically, when the data is fitted over $T < T_c/3 = 3$ K, the exponent is found $n = 1.8$ for the magnetic field applied along c and 1.7 for the field in the perpendicular direction. These values do not change when the fitting interval is reduced to $T < T_c/6 = 1.5$ K for example, and the same sub- T^2 behaviour is observed in other equivalent samples. In fact, the same sub- T^2 behavior is also observed in the μ SR data which corresponds to the circles in 2 (b).

The linear-in- T behavior at $T \ll T_c$ of the penetration depth of a superconductor with line nodes is well known to become T^2 due to impurity scattering [4, 15]. In the case of a fully gapped superconductor with an unconventional gap structure such as the s_{\pm} one, the exponential behavior also becomes T^2 due to impurity scattering. However, such a possibility is ruled out in our case since we observe an exponent that is always $n \leq 2$. Likewise, an extended s -wave with c -axis line nodes can be ruled out. The sub-quadratic behaviour, however, is compatible with both a s_{\pm} -wave with accidental nodes (or very deep gap minima) or a d -wave with symmetry-imposed nodes.

We note that the measured λ does not display any Curie upturn at low temperatures, which indicates that the observed power-law behavior is due to non-magnetic impurities. The degree of disorder that is introduced by these impurities can be quantified by comparing the zero-temperature coherence length $\xi_0 \simeq 4.3$ nm [11] to the mean-free path ℓ . The latter quantity can be estimated from the measured value of the normal-state conductivity and the one computed from DFT as described in the Methods section, which correctly captures the complex multiband features of our system. Thus, ℓ is estimated to be $\lesssim 5$ nm. According to this estimate, the samples have to be considered in a borderline case between the clean ($\ell \gg \xi_0$) and the dirty limit ($\ell \ll \xi_0$). This obviously makes the quantitative analysis of the data rather involved, which can explain the above limitations related to the μ SR fits and the TDO geometrical factors. In any case, both these data sets display the same sub- T^2 behavior revealing the nodal character of the superconducting gap in LaFeSiH.

DISCUSSION

The 1111 compound LaFeAsO provides a reference electronic structure for the Fe-based superconductors. Here, the Fermi surface displays electron and hole pockets that

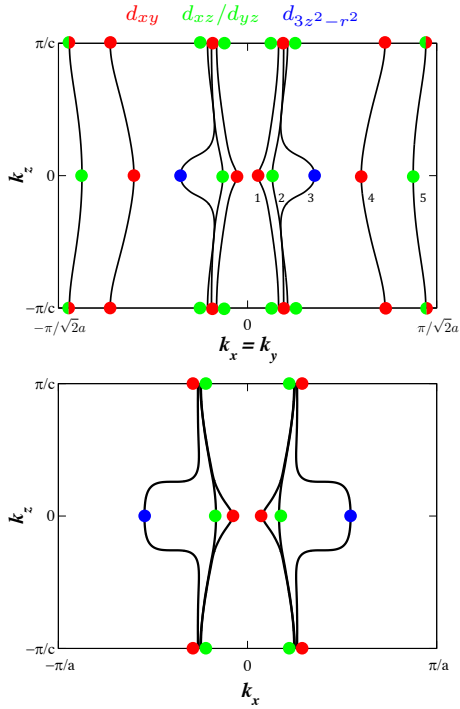


FIG. 3. Fermi surface cuts of LaFeSiH at $k_x = k_y$ (top) and $k_y = 0$ (bottom). The circles indicate the main orbital contributions by the following colors: d_{xy} (red), d_{xz}/d_{yz} (green), and $d_{3z^2-r^2}$ (blue), and the Fermi sheets are numbered in the top panel.

are separated by the wavevector $(\pi, 0)$ (in the 1Fe/unit-cell notation), so that standard considerations on pairing by repulsive interactions suggest a s_{\pm} -wave pair state [5] with a subdominant d -wave channel [7, 17]. In this picture the anisotropy in the s_{\pm} gap function is controlled by several features, notably the 2D vs. 3D character of the Fermi surface and its orbital weights [18, 19]. The strength of the $(\pi, 0)$ interactions, in particular, has a strong dependence on the presence/absence of a $d_{x^2-y^2}$ band near the Fermi level (eventually determined by the actual lattice structure), which then controls the nodeless vs. nodal character of the s_{\pm} state and can even promote the d -wave one [20].

Compared to LaFeAsO, the electronic band structure of LaFeSiH is visibly more 3D as illustrated by the Fermi surface cuts shown in Fig. 3. This is largely due to the prominent dispersion hole pockets —i.e. the inner Fermi-surface sheets 1, 2 and 3— along the c axis. As a result, the overall nesting between electron and hole pockets is drastically deteriorated, which is highly detrimental for the fully gapped s_{\pm} pairing and can introduce accidental nodes [20]. In addition, the $d_{x^2-y^2}$ character of the outer sheets is absent, which also goes in the same direction. The d -wave channel, in contrast, is mainly linked to the electron pockets (sheets 4 and 5) which better retain its propitious features. These considerations support our

experimental finding of a nodal superconducting gap in LaFeSiH, including the comparatively rare d -wave case [6, 21] among the Fe-based superconductors as a possible candidate.

In conclusion, we have determined the magnetic penetration depth of the novel iron-based superconducting silicide LaFeSiH as a function of the temperature in the vortex and in the Meissner state using muon-spin rotation and tunnel-diode oscillators. The observed power-law behavior reveals the presence of low-energy excitations characteristic of nodal superconductivity. The effective zero-temperature value is found to be $\lambda(0) = 336$ nm, in agreement with DFT calculations. The specific features of the electronic band structure of LaFeSiH suggest a prominent role of the electron pockets and accordingly a d -wave superconducting state, even if a s_{\pm} -wave superconducting gap with accidental nodes (or more generally deep gap minima) is also compatible with our experimental findings. This outlines an analogy to the overdoped behavior of previous iron-based superconductors that is expected to motivate further studies.

METHODS

Sample preparation

The LaFeSiH powder sample for the TF- μ SR experiment was obtained as described in [11]. From this powder, small single-crystals were singled out for the TDO measurements. The geometry of the selected crystals corresponds to the slab geometry with typical thicknesses $2d \sim 10\mu\text{m}$ in the c direction and planar dimensions $2w \sim 300\mu\text{m}$.

μ SR experiment and analysis

The μ SR experiment was carried out using the MuSR spectrometer at ISIS Facility, UK. Thus, we measured the muon spin depolarization that results from the application of a magnetic field of 30 mT ($> H_{c1}$, see [11]) in the transverse-field configuration (TF- μ SR). The depolarization rate has a component due to the nuclear magnetic contributions of the sample. In addition, if the sample is a type-II superconductor, the depolarization rate is expected to develop an extra contribution due to the inhomogeneous distribution of magnetic field in the vortex state [13], which is directly linked to the magnetic penetration depth λ . Thus, in the simplest case, the TF- μ SR asymmetry spectrum can be modeled as [13, 14]

$$A(t) = A_s e^{-\sigma^2 t^2/2} \cos(\omega_s t + \theta) + A_{bg} \cos(\omega_{bg} t + \theta). \quad (1)$$

The first term in this expression describes the oscillations (with relaxation) produced by the sample while the second accounts for the background oscillations (without relaxation) due to e.g. the Ag-sample holder, with θ is the phase which is related to the detector geometry. In the first term, the total depolarization rate σ reads $\sigma = \sqrt{\sigma_{\text{nm}}^2 + \sigma_{\text{sc}}^2}$ where σ_{nm} and σ_{sc} represent

the aforementioned nuclear and superconducting vortex-lattice contributions respectively. Furthermore, for a triangular vortex-lattice in a type-II superconductor such that $\kappa = \lambda/\xi \gg 70$ and $0.13/\kappa^2 \ll H/H_{c2} \ll 1$, the superconducting part reduces to $\sigma_{\text{sc}}^2 = 3.71 \times 10^{-3} \frac{\gamma_\mu^2 \phi_0^2}{\lambda^4}$, where γ_μ is the muon gyromagnetic ratio and ϕ_0 is the flux quantum [13, 22, 23].

The σ_{sc} obtained in this way is therefore directly related to λ , which we further exploited to determine the superconducting gap Δ and the pairing symmetry. The temperature dependence of σ_{sc} , in particular, is such that $\frac{\sigma_{\text{sc}}(T)}{\sigma_{\text{sc}}(0)} = \frac{\lambda^{-2}(T)}{\lambda^{-2}(0)}$. This ratio is customarily modeled within the London approximation as

$$\frac{\sigma_{\text{sc}}(T)}{\sigma_{\text{sc}}(0)} = 1 + \frac{1}{\pi} \int_0^{2\pi} \int_{\Delta(T, \phi)}^{\infty} \left(\frac{\partial f}{\partial E} \right) \frac{EdEd\phi}{\sqrt{E^2 - \Delta(T, \phi)^2}} \quad (2)$$

for s - and d -wave superconductors, where $f = [1 + \exp(E/k_B T)]^{-1}$ is the Fermi function and ϕ is the azimuthal angle across the Fermi surface. Here the superconducting gap function is conveniently expressed as $\Delta(T, \phi) = \Delta_0 \Gamma(T/T_c) g(\phi)$. Thus, its temperature dependence can be taken as $\Gamma(T/T_c) = \tanh\{1.82[1.018(T_c/T - 1)]^{0.51}\}$, while its angular dependence can be assumed to be $g(\phi) = 1$ for an isotropic s -wave gap, $g(\phi) = \frac{1+\alpha \cos 4\phi}{2}$ for an anisotropic one, and $g(\phi) = |\cos(2\phi)|$ for d -wave gap with line nodes for example [14, 24]. This model is readily extended to the multi-gap case.

TDO measurements

We used a high stability LC oscillator with resonant frequency 13 MHz driven by a tunnel diode in a ^3He refrigerator. Thus, we measured the relative shift of the resonant frequency $\Delta f/\Delta f_0$ which is directly related to the AC magnetic susceptibility χ' and hence $\Delta\lambda(T) \equiv \lambda(T) - \lambda(0)$ (here Δf_0 is the frequency shift obtained when the sample is completely extracted from the coil at the base temperature, while the factor of proportionality is defined by the TDO effective dimension of the sample) [15, 24–26].

The geometry of the measured crystals corresponds to the slab geometry with typical thicknesses $2d \sim 10\mu\text{m}$ in the c direction and planar dimensions $2w \sim 300\mu\text{m}$. Thus, the TDO effective sample dimension is expected to be $\sim 0.2w$ when the magnetic field is applied along the c axis and $\sim d$ when it is perpendicular to c [27]. Furthermore, if $H \parallel c$ then the screening supercurrents flow entirely in the ab -plane and hence the in-plane penetration depth λ_{ab} is probed. However, if $H \perp c$ the screening is due to supercurrents flowing both in-plane and out-of-plane so that the mixture $\lambda_{ab} + \frac{d}{w}\lambda_c$ containing the contribution due to the out-of-plane penetration depth λ_c is probed.

DFT calculations

We performed DFT calculations using the FLAPW method as implemented in the WIEN2K package [28] with the PBE exchange-correlation functional [29]. Specifically, we considered the low-temperature structure reported of LaFeSiH in [11], with muffin-tin radii of 2.30, 2.10, 2.20 and 1.20 a.u for La, Fe, Si and H atoms respectively, and a plane-wave cutoff $R_{mt}K_{max} = 5.0$ in our spinless calculations. The integration over the Brillouin zone was performed using a $15 \times 15 \times 7$ k -mesh, while the Fermi velocity was computed using a denser $64 \times 64 \times 32$ k -mesh as $\mathbf{v} = \mathbf{p}/m_e$ with \mathbf{p} being the expectation value of the momentum operator and m_e the electron mass.

From these calculations we further computed the penetration depth in the London approximation according to the formula $(\lambda_{ij}^2)^{-1}(0) = \frac{\mu_0 e^2}{4\pi^3 \hbar} \oint_{FS} dS \frac{v_i v_j}{|\mathbf{v}|}$ (see e.g. [15, 27]). Here \mathbf{v} is the Fermi velocity and the integral is over the Fermi surface. In these calculations In addition, we also computed the conductivity in the relaxation-time approximation which reads $\sigma_{ij} = (e^2 \tau / \Omega_0) \int_{BZ} v_i(\mathbf{k}) v_j(\mathbf{k}) \delta(\varepsilon(\mathbf{k}) - \varepsilon_F) d\mathbf{k}$ within the Boltzmann transport theory [30]. Here Ω_0 is the volume of the first Brillouin zone and the relaxation time τ gives the mean-free path as $\ell = v_F \tau$.

ACKNOWLEDGEMENTS

P.R., F.B., J.B.V., S.T., and A.C. are supported by the Grant ANR-18-CE30-0018-03 IRONMAN. DTA and ADH acknowledge financial assistance from CMPC-STFC grant number CMPC-09108. AB would like to acknowledge the Department of Science and Technology (DST) India, for an Inspire Faculty Research Grant (DST/INSPIRE/04/2015/000169), and the UK-India Newton grant for funding support. We would like to thank G. Stenning and D. Nye for their help in the sample characterization and the ISIS Facility for proving beam time on the MuSR spectrometer, DOI: 10.5286/ISIS.E.RB1900103.

* devashibhai.adroja@stfc.ac.uk
 † andres.cano@cnrs.fr

[1] M. Tinkham, *Introduction to Superconductivity* (Dover Publications, 2004).
 [2] H. Hosono and K. Kuroki, *Physica C: Superconductivity and its Applications* **514**, 399 (2015).
 [3] P. J. Hirschfeld, M. M. Korshunov, and I. I. Mazin, *Reports on Progress in Physics* **74**, 124508 (2011).
 [4] P. J. Hirschfeld, *C. R. Phys.* **17**, 197 (2016).
 [5] I. I. Mazin, D. J. Singh, M. D. Johannesson, and M. H. Du, *Phys. Rev. Lett.* **101**, 057003 (2008).
 [6] K. Kuroki, S. Onari, R. Arita, H. Usui, Y. Tanaka, H. Kontani, and H. Aoki, *Phys. Rev. Lett.* **101**, 087004 (2008).
 [7] S. Graser, T. A. Maier, P. J. Hirschfeld, and D. J. Scalapino, *New Journal of Physics* **11**, 025016 (2009).
 [8] S. Maiti, M. M. Korshunov, T. A. Maier, P. J. Hirschfeld, and A. V. Chubukov, *Phys. Rev. Lett.* **107**, 147002 (2011).
 [9] Y. Mizukami, M. Konczykowski, Y. Kawamoto, S. Kurata, S. Kasahara, K. Hashimoto, V. Mishra, A. Kreisel, Y. Wang, P. J. Hirschfeld, Y. Matsuda, and T. Shibauchi, *Nature Communications* **5**, 5657 EP (2014).
 [10] Z. Guguchia, A. Amato, J. Kang, H. Luetkens, P. K. Biswas, G. Prando, F. von Rohr, Z. Bukowski, A. Shengelaya, H. Keller, E. Morenzoni, R. M. Fernandes, and R. Khasanov, *Nature Communications* **6**, 8863 EP (2015).
 [11] F. Bernardini, G. Garbarino, A. Sulpice, M. Núñez Regueiro, E. Gaudin, B. Chevalier, M.-A. Méasson, A. Cano, and S. Tencé, *Phys. Rev. B* **97**, 100504 (2018).
 [12] L. Hung and T. Yildirim, *Phys. Rev. B* **97**, 224501 (2018).
 [13] J. E. Sonier, J. H. Brewer, and R. F. Kieff, *Rev. Mod. Phys.* **72**, 769 (2000).
 [14] A. Bhattacharyya, D. T. Adroja, M. Smidman, and V. K. Anand, *Science China Physics, Mechanics & Astronomy* **61**, 127402 (2018).
 [15] R. Prozorov and V. G. Kogan, *Phys. Rev. B* **74**, 124505 (2011).
 [16] V. Fesenko, V. Gorbunov, and V. Smilga, *Physica C: Superconductivity* **176**, 551 (1991).
 [17] K. Kuroki, S. Onari, R. Arita, H. Usui, Y. Tanaka, H. Kontani, and H. Aoki, *Phys. Rev. Lett.* **101**, 087004 (2008).
 [18] T. A. Maier, S. Graser, D. J. Scalapino, and P. J. Hirschfeld, *Phys. Rev. B* **79**, 224510 (2009).
 [19] R. Sknepnek, G. Samolyuk, Y.-b. Lee, and J. Schmalian, *Phys. Rev. B* **79**, 054511 (2009).
 [20] K. Kuroki, H. Usui, S. Onari, R. Arita, and H. Aoki, *Phys. Rev. B* **79**, 224511 (2009).
 [21] J. D. Fletcher, A. Serafin, L. Malone, J. G. Analytis, J.-H. Chu, A. S. Erickson, I. R. Fisher, and A. Carrington, *Phys. Rev. Lett.* **102**, 147001 (2009).
 [22] A. Amato, *Rev. Mod. Phys.* **69**, 1119 (1997).
 [23] E. H. Brandt, *Phys. Rev. B* **68**, 054506 (2003).
 [24] A. Carrington and F. Manzano, *Physica C: Superconductivity and its Applications* **385**, 205 (2003).
 [25] F. Manzano, A. Carrington, N. E. Hussey, S. Lee, A. Yamamoto, and S. Tajima, *Phys. Rev. Lett.* **88**, 047002 (2002).
 [26] P. Diener, P. Rodière, T. Klein, C. Marcenat, J. Kacmarcik, Z. Pribulova, D. J. Jang, H. S. Lee, H. G. Lee, and S. I. Lee, *Phys. Rev. B* **79**, 220508 (2009).
 [27] R. Prozorov and R. W. Giannetta, *Superconductor Science and Technology* **19**, R41 (2006).
 [28] P. Blaha, K. Schwarz, G. Madsen, D. Kvasnicka, J. Luitz, R. Laskowski, F. Tran, and L. D. Marks, WIEN2k, An Augmented Plane Wave + Local Orbitals Program for Calculating Crystal Properties (Karlheinz Schwarz, Techn. Universitt Wien, Austria), 2018. ISBN 3-9501031-1-2.
 [29] J. P. Perdew, K. Burke, and M. Ernzerhof, *Phys. Rev. Lett.* **77**, 3865 (1996).
 [30] P. B. Allen, W. E. Pickett, and H. Krakauer, *Phys. Rev. B* **37**, 7482 (1988).